

# Tuning Strain Sensor Performance via Programmed Thin-Film Crack Evolution

Juan Zhu, Xiaodong Wu, Jasmine Jan, Shixuan Du, James Evans, and Ana C. Arias\*

Cite This: *ACS Appl. Mater. Interfaces* 2021, 13, 38105–38113

Read Online

ACCESS |



Metrics &amp; More



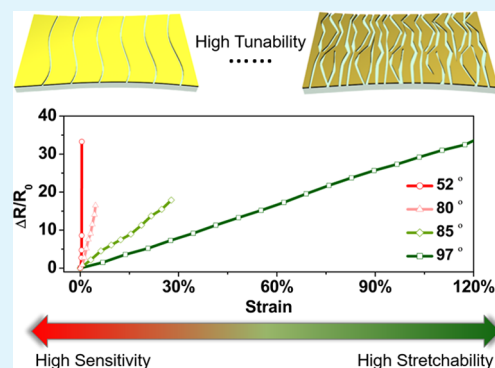
Article Recommendations



Supporting Information

**ABSTRACT:** Stretchable strain sensors with well-controlled sensitivity and stretchability are crucial for applications ranging from large deformation monitoring to subtle vibration detection. Here, based on single-metal material on the elastomer and one-pot evaporation fabrication method, we realize controlled strain sensor performance via a novel programmable cracking technology. Specifically, through elastomeric substrate surface chemistry modification, the microcrack generation and morphology evolution of the strain sensing layer is controlled. This process allows for fine tunability of the cracked film morphology, resulting in strain sensing devices with a sensitivity gauge factor of over 10 000 and stretchability up to 100%. Devices with a frequency response up to 5.2 Hz and stability higher than 1000 cycles are reported. The reported strain sensors, tracking both subtle and drastic mechanical deformations, are demonstrated in healthcare devices, human–machine interaction, and smart-home applications.

**KEYWORDS:** strain sensor, tunability, stretchability, programmed crack, wearable electronics



## 1. INTRODUCTION

Stretchable strain sensors that enable the real-time analysis of mechanical deformations are motivated by the emerging demand for wearable devices and artificial intelligence.<sup>1–14</sup> Different applications require sensors with different and well-defined characteristics including stretchability and sensitivity. Specifically, for applications such as hand gesture recognition, sports monitoring, and home automation, strain sensors with high stretchability and moderate sensitivity are highly desired for stable and reliable signal output. On the contrary, for subtle vibration detection, sensitive electronic skin, and weak physiological signal monitoring, high sensitivity is essential for the sensors to capture subtle signals.

To meet these requirements, efforts have been made to achieve strain sensors with high stretchability or high sensitivity. Highly stretchable sensors have been realized in some systems, such as carbon nanotube film strain sensors,<sup>15–17</sup> silver nanowire-elastomer nanocomposite strain sensors,<sup>18</sup> fiber-shaped strain sensors,<sup>19</sup> and capacitive-type strain sensors,<sup>20</sup> but their sensitivity is not high enough for further applications in small deformation detection. Strain sensors with high sensitivity can also be achieved by intentionally generating channel cracks on rigid metal films to design highly sensitive electronic skins.<sup>21–23</sup> Such cracked systems can only function in a strain range of less than 10%. Microcrack-based strain sensors with improved stretchability by replacing the metal film with composite materials have been reported.<sup>24–26</sup> However, most microcracked sensors structured

on composite materials sacrifice their high sensitivity at a small strain range (<10%), which plays a critical role in capturing abundant signals of weak activities (such as wrist pulse, throat vibration, etc.). Therefore, the development of multifunctional strain sensors with highly tunable stretchability and sensitivity based on a simple material system and efficient approach is highly desired yet not reported.

Motivated by the tradeoffs between sensitivity and stretchability of the existing strain sensing devices, here we present highly tunable strain sensors based on a programmed crack evolution process. Specifically, by adjusting the surface wettability of the elastomer underneath, which support the gold (Au) strain sensing layer, we can generate a wide range of cracking morphologies (from cracked domains to cut-through cracks) within the Au layer. Tuning of cracking morphologies in the metal layer allows for programming high stretchability for the sensor with high-crack density of cracked domains (over 100%) and high sensitivity for the sensor with low-crack density of cut-through cracks (gauge factor (GF) > 10 000). These strain sensors with well-defined sensitivity and stretchability are fabricated by adjusting the substrate surface

Received: June 12, 2021

Accepted: July 22, 2021

Published: August 3, 2021



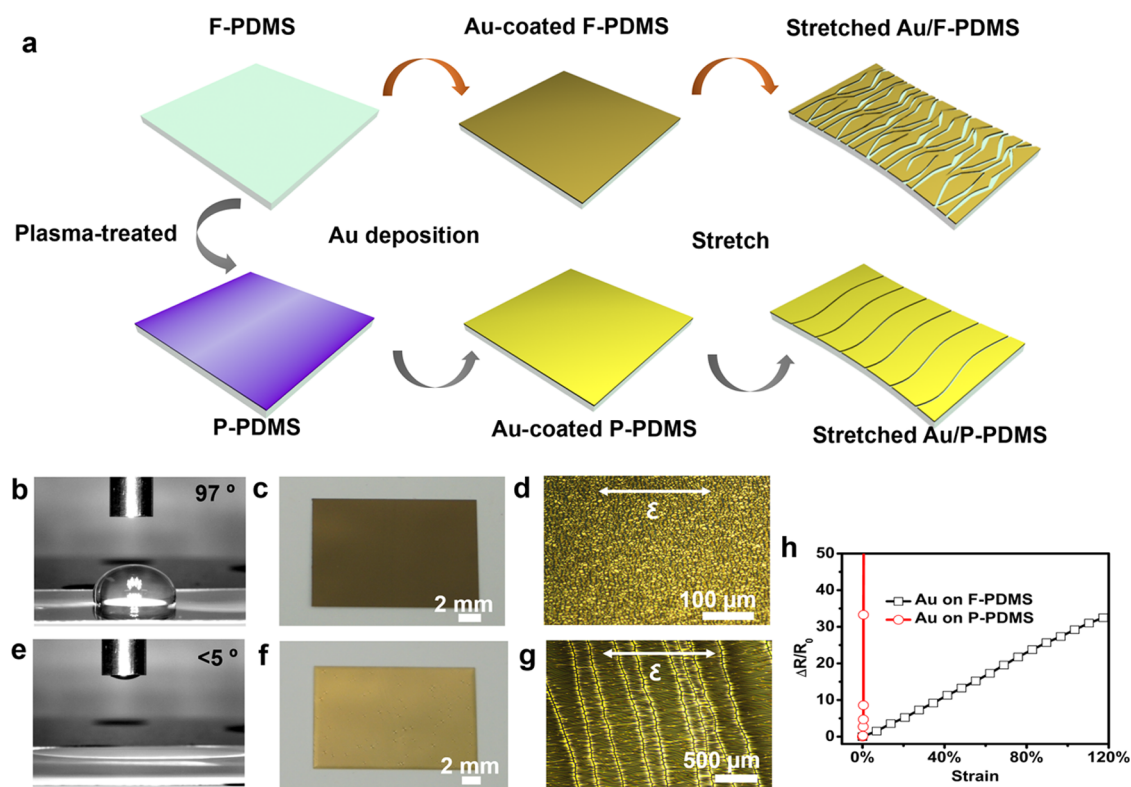


**Figure 1.** Fabrication process and characterization of strain sensors based on programmed Au crack evolution. (a) Schematic for the fabrication process of strain sensors. (b) Water contact angle image of fresh PDMS (F-PDMS). (c) Photo of the Au film deposited on F-PDMS. (d) Microscope image of Au cracked domains on F-PDMS under a tensile strain of 100%. (e) Water contact angle image of plasma-treated PDMS (P-PDMS) under 50 W for 120 S. (f) Photo of the Au film on P-PDMS. (g) Microscope image of Au cut-through cracks on P-PDMS under a tensile strain of 5%. (h) Relative resistance changes of strain sensors structured on Au/F-PDMS and Au/P-PDMS with respect to the applied strain up to 120%. The white arrows in (d) and (g) show the direction of the applied strain.

chemistry and made from a single-metal sensing material evaporated from one pot, which greatly simplifies the fabrication process while maintaining the sensor multifunctionality. In addition to simple fabrication, our sensors exhibit high tunability, good sensitivity, high stretchability, cyclic stability, and fast dynamic response. We also demonstrate a wide spectrum of practical applications of the sensors, such as smart control of light-emitting diode (LED) light intensity, hand gesture recognition, elbow bending, bicycling monitoring, subtle physiological activity detection, and sound vibration monitoring. The programmable cracking technology reported here may serve as a powerful and general strategy to design multifunctional and versatile soft electronics systems.

## 2. RESULT AND DISCUSSIONS

**2.1. Structural Design of Strain Sensors Based on Programmed Au Crack Evolution.** A conductive metal film supported on an elastomer is investigated in this work. The brittle metal film will crack when the underlying elastomer is subjected to a tensile strain due to the different modulus mismatch between the metal film and elastomer. The emergence of the cracks in the metal film results in changes in the film conductivity. First, poly(dimethylsiloxane) (PDMS) precursor is spin-coated on a poly(ethylene naphthalate) (PEN) carrier, followed by curing to form a thin and uniform elastomer film (with a thickness of around 100  $\mu\text{m}$ ). This thin elastomer layer with high softness provides a good conformal factor to the human body and thus can improve the signal-to-

noise ratio (SNR) for physiological activity monitoring. Prior to spin-coating, the PEN film is attached to a glass slide using a Gel-Pak film for simpler handling and subsequently removed for the metal deposition. Figure 1a is a schematic of the fabrication process for the strain sensors. A film of 50 nm thick Au is deposited directly on fresh PDMS (F-PDMS) or plasma-treated PDMS (P-PDMS) using thermal evaporation. The F-PDMS surface shows a relatively low surface energy with a water contact angle around  $97^\circ$  (Figure 1b). Plasma treatment increases the surface energy of P-PDMS as shown by the lower water contact angle to below  $5^\circ$  (Figure 1e). The different surface wettabilities of PDMS indicated by contrasting water contact angles can affect the subsequent growth of the Au film. The differences in the metal films can be seen easily from the contrasting colors of the Au film-coated F-PDMS (Figure 1c) and Au film-coated P-PDMS (Figure 1f). Compared with Au-coated F-PDMS, which has a dark-brown color, the Au-coated P-PDMS surface shows a more shiny and metallic color. These visible color differences result from the variation in the particle size of the Au film on the PDMS as a result of the different surface chemistries. Upon the stretching of the F-PDMS underneath, the Au film on F-PDMS breaks into plenty of isolated microcracked domains (Figure 1d). In comparison, the metal film on P-PDMS fractures into cut-through cracks with a lower crack density when subjected to the same tensile strain (Figure 1g). The crack morphology evolution in the metal film deposited on PDMS with tunable surface energy allows the corresponding sensors to achieve specific sensitivity and stretchability. In this study, sensitivity is defined as gauge

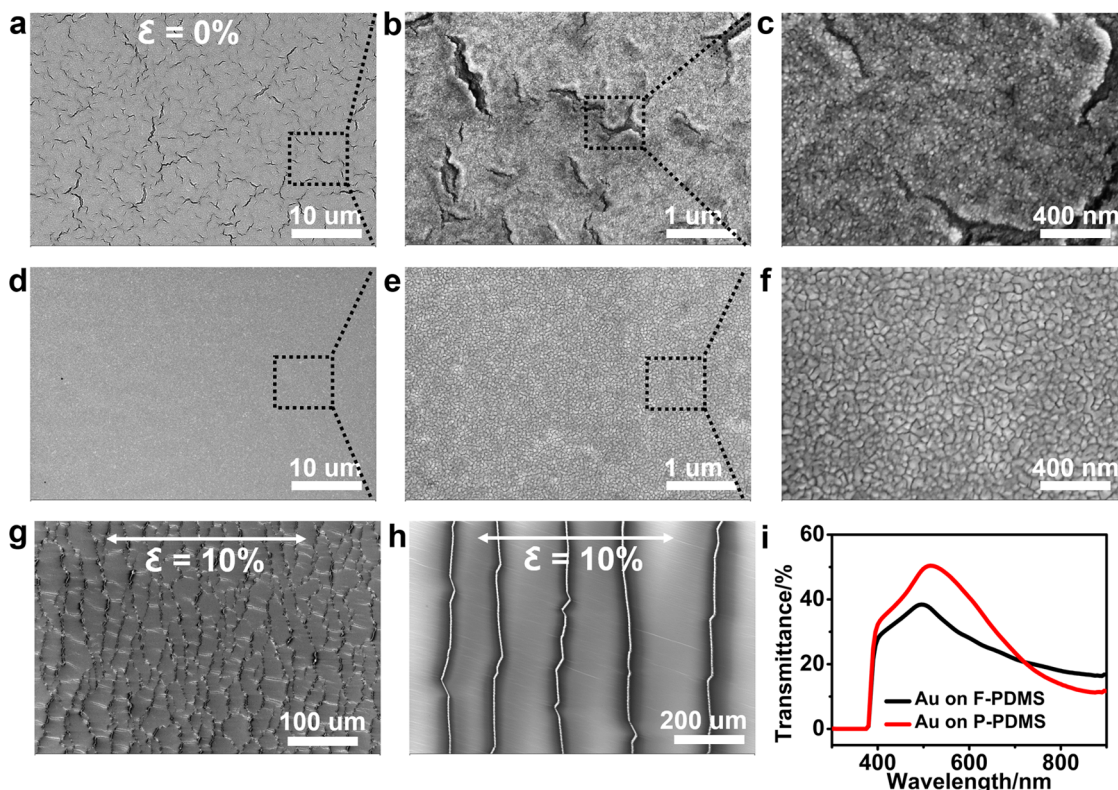


**Figure 2.** Characterization of strain sensors. (a–c) SEM images of the Au film on unstretched F-PDMS at various magnifications. (d–f) SEM images of the Au film on unstretched P-PDMS at various magnifications. (g) SEM image of the Au film on F-PDMS at a tensile strain of 10%. (h) SEM image of the Au film on P-PDMS at a tensile strain of 10%. (i) UV–vis spectra of the unstretched Au film on F-PDMS and P-PDMS.

factor (GF) =  $\Delta R/(R_0\varepsilon)$ , where  $\Delta R$  is the change in electrical resistance,  $R_0$  is the initial electrical resistance, and  $\varepsilon$  is the tensile strain; stretchability ( $\varepsilon_{\text{limit}}$ ) is defined as the value of tensile strain at which the crack sensors lose their conductivity. The strain sensor with Au-coated F-PDMS can realize stretchability over 100%. The sensitivity for the sensor can be greatly enhanced (GF increases from 30 to over 10 000) with the improved wettability of the P-PDMS surface (Figure 1h). Materials, fabrication techniques, working range, and gauge factor of microcrack-based sensors reported in the literature and in this paper are summarized in Table S1. The sensors in this work are made from single-metal material on the elastomer and fabricated by one-pot evaporation, could function in strain range of up to 100%, and realize gauge factor over 1000.

**2.2. SEM and UV–vis Spectra Characterization of Strain Sensors.** Two typical types of strain sensors are further characterized by scanning electron microscope (SEM). From the SEM images at different magnifications in Figure 2a–c, the Au film on unstretched F-PDMS already has visible cracked domains before the stretching. On the other hand, the metal film on unstretched P-PDMS displays a more uniform, compact, and smoother surface (Figure 2d–f). This can be understood through the capillary theory of heterogeneous nucleation, which relates the substrate's surface energy with film growth modes.<sup>27,28</sup> In this work, plasma exposure creates dangling bonds at the surface of the P-PDMS, providing activation energy for enhanced bonding between the metal film and the substrate. This favors a layer growth mode, and as a result, the deposited metal film on P-PDMS will exhibit a smoother film compared to that of the F-PDMS, which prefers

an island growth mode and exhibits intrinsic cracks. When the F-PDMS substrate is subject to a tensile strain, the metal film with intrinsic cracked domains will continue to fracture into isolated cracked domains. Cracked domains in the Au film on F-PDMS are observed at a tensile strain of 10% (Figure 2g). As a comparison, Figure 2h shows the distinguishing cut-through cracks in the Au film supported on P-PDMS when subjected to the same strain. We deposited 12 nm Au on F-PDMS and P-PDMS and characterized transmittance using UV–vis spectra. The transmittance peak of the Au film on the P-PDMS with higher hydrophilicity exhibits a red shift and the Au film is more transparent compared to that on F-PDMS with lower hydrophilicity (Figure 2i). Red shift in the Au film on P-PDMS is consistent with larger grain size in the Au film compared to that on F-PDMS, which could also be clearly verified from magnified SEM images in Figure 2c,f. The surface energy of PDMS depicted as water contact angle ( $\theta_c$ ) could be further finely controlled by adjusting the time of oxygen plasma treatment ( $T_p$ ) (Figure S1), which allows metal film morphologies with more variability on PDMS. SEM images and UV–vis spectra of Au films on P-PDMS with multiple  $\theta_c$  (97, 85, 75, 52°) in Figure S2 show the high tunability of the technique. The schematic for metal film growth mode (i.e., island growth, layer growth, and combination growth) explains the mechanism for the formation of different metal film formation on PDMS with varied  $\theta_c$  (Figure S2). The crack density has a notable effect on sensor performances including the stretchabilities and sensitivities. The crack morphologies of Au films on PDMS with different  $\theta_c$  (97, 85, 80, 52°) under a tensile strain of 5% are investigated (Figure S3) and the crack density in the Au film on PDMS with various  $\theta_c$  are counted in

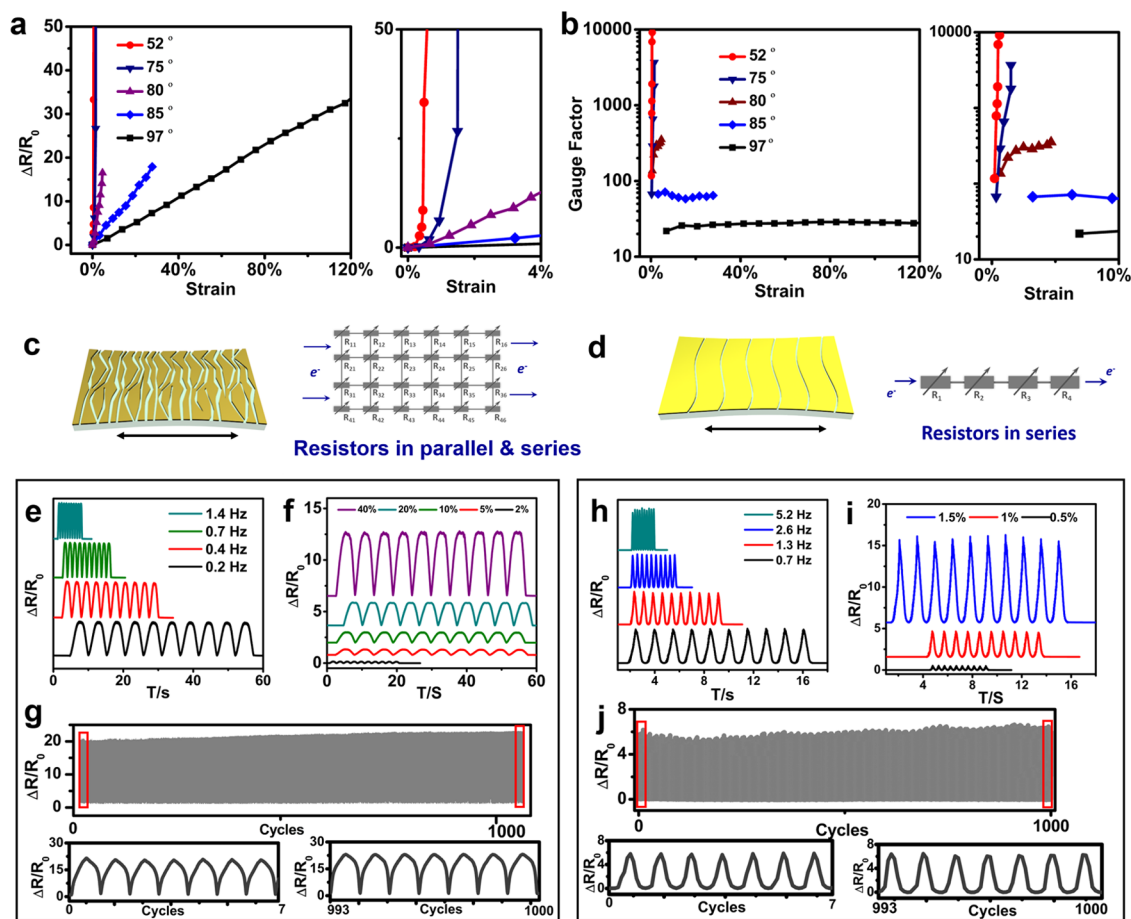


**Figure 3.** Sensor performance of tunable strain sensors. (a) Relative resistance changes of strain sensors tuned by different water contact angles of PDMS versus the applied strain up to 120% (the left graph) and 4% (the right graph). (b) Corresponding gauge factors of strain sensors versus the applied strain up to 120% (the left graph) and 10% (the right graph). (c, d) Schematic showing the mechanism for resistance changes of sensors with Au cracked domains and Au cut-through cracks. (e–g) Performance of the sensor with cracked domains, constructed by the Au film on F-PDMS with 97° water contact angle. (e) Frequency test under the tensile strain from 0 to 5%. (f) Reversible loading–unloading behavior for various strains, from 2 to 40%. (g) Loading–unloading performance during a cyclic test for 1000 cycles under an applied strain of 50% at a frequency of 0.2 Hz. (h–j) Performance of the sensor with cut-through cracks, structured by Au films on PDMS with 75° water contact angle. (h) Frequency test under the tensile strain from 0 to 1.5%. (i) Reversible loading–unloading behavior for various strains, from 0.5 to 1.5%. (j) Loading–unloading performance of the strain sensor during a cyclic test for 1000 cycles under an applied strain of 1% at a frequency of 1 Hz.

**Figure S4.** The cracking mechanism for different Au structures on PDMS with varied  $\theta_c$  is displayed in **Figure S5**. We observed that in more compact Au film, deposited on P-PDMS, a traversing crack is formed under applied strain after breaking at the neck. However, for the Au film on F-PDMS with intrinsic cracked domains, the tensile force will redistribute and cannot propagate in a cut-through direction when it meets the boundaries of cracked domains. In other words, the tensile stress is concentrated on the intrinsic cracked domains in the unstretched Au film on F-PDMS and results in the further evolution of the original cracked domains. The present mechanism for cracked-domain evolution in the Au film with intrinsic cracks is consistent with the published results for stretchable Au films and Au nanoparticle thin film.<sup>29,30</sup> This technique uses plasma treatment to tune the surface energy of PDMS, which subsequently affects the growth mode, intrinsic cracked domains, and particle size of the Au film. This results in Au films with distinctive microcrack morphologies and performances under strain. This mechanism in this work is different from the microcracked sensors structured on carbon composite/PDMS tuned by plasma treatment,<sup>24,25</sup> where the sensors need to be prestretched to a

critical straining (100%) and microcracks were generated through stress transfer from exposed polymer substrates to the composite thin films. Our tuning results are analogous to adjusting the interaction force between the sensing metal and the elastomer by introducing another metal film as an adhesive layer prior to the deposition of a sensing metal film.<sup>22</sup> However, in our technique, only one vacuum-deposited material is required, which enables multifunctional devices from one deposition process. Such one-step deposition greatly simplifies the fabrication process and realizes energy savings. The crack morphology evolutions are also investigated for multiple sensors under increasing tensile strain (**Figures S6 and S7**). Different materials and growth techniques are also investigated in the work. Unlike the Au film, aluminum (Al) film did not show differences with/without plasma treatment and the devices structured on the Al film lost their conductivity when subjected to a small strain <10%. Platinum (Pt) film was reported to have cut-through cracks on fresh poly(urethane acrylate) (PUA), which is also different from the Au film.<sup>21</sup> Dissimilar to the Au film deposited by thermal evaporation in our work, the Au film on F-PDMS grown by electron beam evaporation was reported to have cut-through cracks.<sup>22</sup>

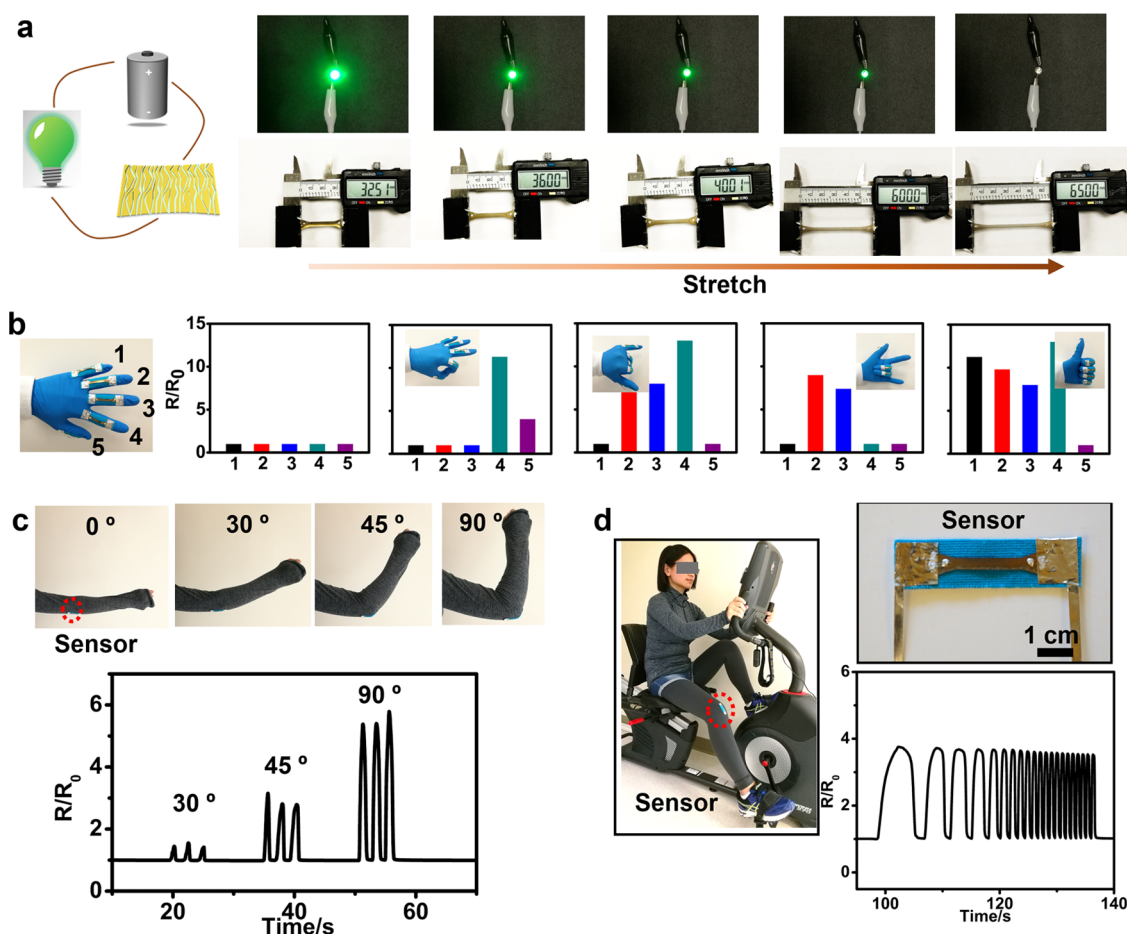


**Figure 4.** Application demonstrations of stretchable strain sensors with cracked domains. (a) LED light intensity is controlled by the strain sensor. An LED is connected in series with the strain sensor under 2.6 V source voltage. (b) Recognition of hand gestures. (c) Signals from the elbow bending at a certain angle. (d) Bicycling at different frequencies.

**2.3. Sensor Performance Characterization of Tunable Strain Sensors.** We further show that the strain sensing performance can be programmed by modulating the surface energy of the PDMS substrate. We investigate how sensitivity and stretchability limit ( $\epsilon_{\text{limit}}$ ) would be affected by the water contact angle ( $\theta_c$ ) of PDMS. As displayed in Figure 3a, the stretchability of the sensor is reduced with respect to increased surface energy (i.e., decreased  $\theta_c$ ) of PDMS. The results show that  $\epsilon_{\text{limit}}$  changes from over 120% at  $\theta_c = 97^\circ$ , to around 27% at  $\theta_c = 85^\circ$ , 4.5% at  $\theta_c = 80^\circ$ , 1.5% at  $\theta_c = 75^\circ$ , 0.6% at  $\theta_c = 52^\circ$  or lower. Sensor sensitivity is greatly improved with a higher surface energy of PDMS, shown in Figure 3b. The developed strain sensors achieve GFs over 30 ( $120\% > \epsilon > 27\%$ ), 60 ( $27\% > \epsilon > 4.5\%$ ), 200 ( $4.5\% > \epsilon > 1.5\%$ ), 600 ( $1.5\% > \epsilon > 0.3\%$ ), and 100 ( $0.3\% > \epsilon$ ). The highest achieved GFs for our sensor were over 10 000. The precise and wide-range tunability of GFs from 30 to over 10 000 in the strain range from 0 to 120% is in contrast with previous reported cracked systems, which allow a high sensitivity range ( $\text{GF} > 2000$ ) but only with a limited stretchability ( $\epsilon_{\text{limit}} < 5\%$ ).<sup>21,22</sup> The initial resistance of Au films on PDMS with varied  $\theta_c$  is shown in Figure S8. The statistical information for the sensors' performances is summarized in Figure S9 to show the uniformity and accuracy of this method. To show the effects of the surface energy of PDMS on the sensor performances clearly, maximum stretchabilities and sensitivities of the sensors with respect to the water contact angles of PDMS are summarized in Figure

S10. A schematic illustration is used to show the mechanism for the resistance change of crack sensors upon stretching (Figure 3c). As previously discussed, the metal film supported on the F-PDMS with a low surface energy will break into many isolated cracked domains upon stretching, and thus the metal film could be equivalent to small resistors connected in parallel and in series (Figure 3c). Some of the resistors will gradually lose the connections at increasing strain, eliminating electrical pathways for electrons. However, many of the connections remain intact (i.e., the metal film is still conductive at a comparably large strain). The metal film on the P-PDMS is dominated by cut-through cracks with a low density at the applied strain and can be regarded as being composed of resistors connected in series (Figure 3d). The resistors will disconnect easily and, as a result, the metal film will quickly lose conductivity at a small strain, i.e., such strain sensors have a smaller stretchability compared to the sensors based on the metal film on F-PDMS.

The performance of well-defined strain sensors based on cracked domains and cut-through cracks is thoroughly characterized (Figure 3e–j). The strain sensing devices with cracked domains are tested at frequencies of 0.2–1.4 Hz at the applied strain of 5%, and sensors with cut-through cracks are measured at 0.7–5.2 Hz at the applied strain of 1.5%. Both kinds of sensors show an accurate response independent of the test frequency, as displayed in Figure 3e,h separately. Reversible loading–unloading behaviors for various strains

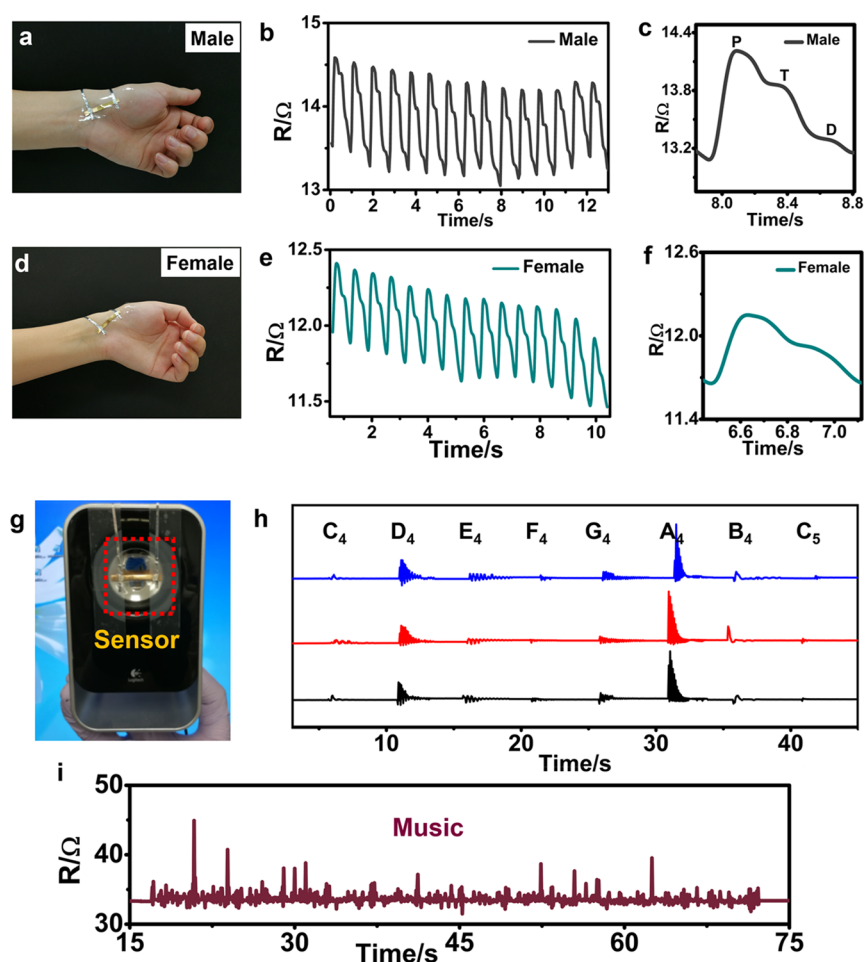


**Figure 5.** Applications of strain sensors with cut-through cracks for detecting subtle human physiological activities and sound vibrations. (a–f) Detection of the wrist pulse signal from a male subject (a–c) and a female subject (d–f). (g–i) Cracked-domain strain sensor attached to a loudspeaker diaphragm for sound recognition. (g) Image of a strain sensor attached to a loudspeaker. (h) Different tones of piano played from the loudspeaker produce various wave functions, which were collected using the cracked-domain sensor. The multiple measurements show the good repeatability of the sensor. (i) Measurement for sound waves of music playing.

are investigated and shown in Figure 3f,i. The strain ranges applied are from 2 to 40% for the strain sensors with cracked domains and 0.5–1.5% for the sensitive sensors with cut-through cracks, demonstrating high tunability of this technique. The sensor fabricated with Au films deposited on plasma-treated PDMS for a different exposure time (15 s) is tested at frequencies varying from 0.35–2.8 Hz and under strains of 1–10% (Figure S11). The device response is independent of frequency, and repeatability is demonstrated across different applied strains. Cyclic stability of strain sensors is the primary concern for reliable long-term use in practical applications. A strain of 50% is repeatedly applied to the cracked-domain sensor, and a strain of 1% is employed to the cut-through crack sensor for 1000 cycles. The relative resistance changes are recorded in Figure 3g,j, respectively. The small images in Figure 3g,j show magnified signals for the beginning and end of the cycling test. The devices show good stability for 1000 cycles with slightly increased resistance, which is very common in the reported results.<sup>22,29</sup> The slight increase in resistance results from the interfacial rearrangement between the Au thin film and the PDMS substrate. Both kinds of sensors are also investigated for stability at more cycles (5000 cycles for cracked-domain sensor and 3000 cycles for

the cut-through cracked sensor), which are shown in Figures S12 and S13.

**2.4. Application Demonstrations of Stretchable Strain Sensors with Cracked Domains.** Because of their high tunability, sensitivity, stretchability, good reliability, fast response, and facile fabrication, programmed strain sensors can be applied for a wide range of potential applications including human–machine interaction and wearable devices. To demonstrate the capabilities of sensors for monitoring large deformations, several applications using stretchable sensors with cracked domains are explored as follows. First, a stretchable sensor with cracked domains is connected in series to a light-emitting diode (LED). Powered with a source voltage of 2.6 V, the sensor is able to adjust light intensity of the LED with varying applied strains, demonstrating its potential application in smart-home design. Initially, the strain sensor exhibits a resistance of only tens of ohms and works as a conducting wire when the LED is lit. As shown in Figure 4a, the light intensity of LED is gradually attenuated with the resistance upswing of the sensor upon an increasing strain. Once exceeding a maximum stretchability limit, the sensor switches to the OFF state that leads to the extinguishing of the LED.

Another implemented example is mounting stretchable sensors on different joints on the body, such as a finger, elbow, or knee, to detect large body motions. Because the sensor has good stretchability and can conform tightly and comfortably to skin, kinesiology tape is a good candidate to support the stretchable sensor in a wearable stretchable strain sensing application. As shown in Figure 4b, five stretchable sensors are attached to the fingers of a hand and can monitor their response to different hand gestures. The hand gestures (five poses shown) can be tracked and recognized well by monitoring the relative resistance changes. To detect arm bending, we mount the strain sensor on the elbow joint (Figure 4c). The relative resistance change is uniform and repeatable when the elbow is bent at a certain angle, and the angles of the arm bending could be precisely determined in this manner. The strain sensor is further mounted on the knee to monitor the relative resistance change when bicycling at different frequencies (Figure 4d). Distinct waveforms for slow bicycling and fast bicycling can be observed, indicating high sensitivity and quick response of the sensor.

**2.5. Applications of Sensitive Strain Sensors with Cut-Through Cracks.** Strain sensors are further demonstrated for monitoring weak strains, such as sensitive electronic skin applications and sound vibrations. First, the sensitive sensor with cut-through cracks is attached to the radial artery on the wrist (Figure 5a) to detect pulse signals in situ and monitor important physiological signals including systolic and diastolic blood pressure as well as heart rate. The sensor shows repeatable and regular pulse shapes during relaxation with a frequency of 70 beats/min (Figure 5b). As presented in Figure 5c, the close-up of a single pulse peak clearly reveals typical characteristics of the pulse waveform for a 30-year-old male, the percussion wave (P-wave), tidal wave (T-wave), and diastolic wave (D-wave),<sup>31,32</sup> demonstrating the high sensitivity of the sensor. Because females normally have weaker physiological signals that are more elusive than male signals, the sensor is also mounted on a female subject to show its feasibility for use on multiple individuals (Figure 5d). It shows a clear and repeatable pulse with a frequency of 90 beats/min during relaxation in Figure 5e and the magnified cycle in Figure 5f.

Sensitive crack sensors are also able to detect sound vibrations, which are challenging to sense precisely due to the high frequency and minute oscillation amplitude. To demonstrate its feasibility as a sound detector, a cut-through crack sensor is attached to the surface of the diaphragm of a loudspeaker (Figure 5g). The resistance change is continuously recorded as different musical tones from 220 to 523 Hz are played (Figure 5h), showing the sensor could clearly recognize each note with a well-distinguished and reproducible waveform. Time-dependent resistance variations are also measured when the music of "Smooth Criminal" is played in Figure 5i. The reliable recording of waveforms of subtle vibrations at various frequencies demonstrates the high sensitivity and fast dynamic response of our sensors.

### 3. CONCLUSIONS

In summary, a novel strategy of crack programming through facile design to tune the sensitivity and stretchability of cracked strain sensors is proposed. The growth and cracking mechanism of the metal film on elastomer can be programmed by tuning the surface chemistry of the PDMS substrate, allowing for wide control over sensitivity and stretchability for

strain sensors. The cracked domain and cut-through crack sensors can serve as a feasible solution for monitoring a wide range of deformations, from large deformations including smart control of LEDs, hand gesture recognition, elbow bending, and bicycling monitoring, to weak deformation signals including pulse monitoring and sound vibrations. The strain sensors demonstrated in this work are fabricated with simple methods, have high sensitivities, a wide range of stretchabilities, fast response, and good reliability. These qualities open up new avenues for regulating the sensitivity and stretchability of future sensing devices and systems.

## 4. EXPERIMENTAL SECTION

**4.1. Fabrication of Strain Sensor.** One hundred twenty-five micrometer-thick polyethylene naphthalate (PEN) film (Q65HA, Teijin-DuPont) was attached to a glass slide using Gel-Pak and employed as the carrier for holding the PDMS film. PDMS precursor (Dow Corning Sylgard 184; by the weight ratio 10:1 of base and cross-linker) was mixed, stirred, and degassed completely. PDMS precursor was subsequently spin-coated on the PEN substrate at 500 r/min for 1 min with an acceleration of 200 r/min, and finally cured at 90 °C for 20 min. The PDMS film on the PEN substrate was detached from the Gel-Pak and cleaned by Scotch Magic Tape before transfer into the chamber for plasma treatment at 50 W for a specific time. The fresh or plasma-treated PDMS film was transported into the evaporation chamber for 50 nm thick Au deposition. Strain sensors were then laser-cut into dumbbell-shaped structures to maintain stable signals for characterization and measurements.

**4.2. Characterization and Measurements.** The sensor assembly and characterization setup are shown in Figure S14. Galn alloy was used to maintain a stable conductivity at a large strain as it is good as connector for measurements in this setup. The electrical resistance signal of the sensor was measured by a custom setup based on a Vernier caliper and a multimeter. Frequency response and cyclic test were carried out by a custom-made setup on a computer-controlled movable stage and Keithley 2400 Source Meter or Agilent Semiconductor Device Analyzer (B1500A). Microscope images were collected by an optical microscope (Eclipse 50i, Nikon). Scanning electron microscope images were taken on a Zeiss Gemini SEM. UV-vis transmittance spectrum was measured by UV-2600. Human physiological signal monitoring was carried out with informed consent under the approval of the University of California, Berkeley Institutional Review Board, protocol ID number 2020-07-13450.

## ■ ASSOCIATED CONTENT

### Supporting Information

The Supporting Information is available free of charge at <https://pubs.acs.org/doi/10.1021/acsami.1c10975>.

Summary of Figure of merit for our sensor and other crack-based sensors (Table S1); Water contact angle measurement (Figure S1); Additional SEM images and UV-vis spectra of Au films on PDMS (Figure S2); Additional microscope images of Au films on PDMS (Figure S3); Crack densities for Au films on PDMS (Figure S4); Mechanism illustrations for Au cracked-domain and cut-through cracks (Figure S5); Crack morphology evolution of the Au film on F-PDMS (Figure S6); Crack morphology evolution of the Au film on P-PDMS with 85° ( $\theta_c$ ) (Figure S7); Initial resistance of Au films respect to water contact angles of PDMS (Figure S8); Statistical information for the sensors' performances (Figure S9); Maximum stretchability and maximum sensitivity for sensors (Figure S10); Performance of the sensor constructed by the Au film on plasma-treated PDMS for 15 s (Figure S11); Performance of the

cracked-domain sensor during a cyclic test for 5000 cycles under an applied strain of 50% (Figure S12); Performance of the cut-through crack sensor during a cyclic test for 3000 cycles under an applied strain of 1% (Figure S13); and Schematics for the measurement setup (Figure S14) (PDF)

## AUTHOR INFORMATION

### Corresponding Author

Ana C. Arias – Arias Department of Electrical Engineering and Computer Sciences, University of California, Berkeley, California 94720, United States; [orcid.org/0000-0001-6866-5250](https://orcid.org/0000-0001-6866-5250); Email: [acarias@eecs.berkeley.edu](mailto:acarias@eecs.berkeley.edu)

### Authors

Juan Zhu – Arias Department of Electrical Engineering and Computer Sciences, University of California, Berkeley, California 94720, United States; [orcid.org/0000-0003-3341-2215](https://orcid.org/0000-0003-3341-2215)

Xiaodong Wu – Arias Department of Electrical Engineering and Computer Sciences, University of California, Berkeley, California 94720, United States

Jasmine Jan – Arias Department of Electrical Engineering and Computer Sciences, University of California, Berkeley, California 94720, United States

Shixuan Du – Institute of Physics & University of Chinese Academy of Sciences, Chinese Academy of Sciences, Beijing 100190, P. R. China; [orcid.org/0000-0001-9323-1307](https://orcid.org/0000-0001-9323-1307)

James Evans – Arias Department of Electrical Engineering and Computer Sciences, University of California, Berkeley, California 94720, United States

Complete contact information is available at:

<https://pubs.acs.org/10.1021/acsami.1c10975>

### Author Contributions

J.Z. and X.W. contributed equally to this work. The manuscript was written through the contributions of all authors. All authors have given approval to the final version of the manuscript.

### Notes

The authors declare no competing financial interest.

## ACKNOWLEDGMENTS

This work was supported by the National Science Foundation (NSF) under the ECCS Grant no. 1610899, K.C. Wong Education Foundation, and the International Partnership Program of Chinese Academy of Sciences (No. 112111KYSB20160061). J.J. acknowledges funding from the National Science Foundation Graduate Research Fellowship under Grant no. DGE 1752814.

## REFERENCES

- (1) Kim, K. K.; Hong, S.; Cho, H. M.; Lee, J.; Suh, Y. D.; Ham, J.; Ko, S. H. Highly Sensitive and Stretchable Multidimensional Strain Sensor with Prestrained Anisotropic Metal Nanowire Percolation Networks. *Nano Lett.* **2015**, *15*, 5240–5247.
- (2) Li, H.; Wu, K.; Xu, Z.; Wang, Z.; Meng, Y.; Li, L. Ultrahigh-Sensitivity Piezoresistive Pressure Sensors for Detection of Tiny Pressure. *ACS Appl. Mater. Interfaces* **2018**, *10*, 20826–20834.
- (3) Gao, Y.; Li, Q.; Wu, R.; Sha, J.; Lu, Y.; Xuan, F. Laser Direct Writing of Ultrahigh Sensitive SiC-Based Strain Sensor Arrays on Elastomer toward Electronic Skins. *Adv. Funct. Mater.* **2019**, *29*, No. 1806786.

- (4) Gong, S.; Yap, L. W.; Zhu, B.; Zhai, Q.; Liu, Y.; Lyu, Q.; Wang, K.; Yang, M.; Ling, Y.; Lai, D. T. H.; Marzbanrad, F.; Cheng, W. Local Crack-Programmed Gold Nanowire Electronic Skin Tattoos for in-Plane Multisensor Integration. *Adv. Mater.* **2019**, *31*, No. 1903789.

- (5) Amjadi, M.; Kyung, K.-U.; Park, I.; Sitti, M. Stretchable, Skin-Mountable, and Wearable Strain Sensors and Their Potential Applications: A Review. *Adv. Funct. Mater.* **2016**, *26*, 1678–1698.

- (6) Wu, C.; Zeng, S.; Wang, Z.; Wang, F.; Zhou, H.; Zhang, J.; Ci, Z.; Sun, L. Efficient Mechanoluminescent Elastomers for Dual-Responsive Anticounterfeiting Device and Stretching/Strain Sensor with Multimode Sensibility. *Adv. Funct. Mater.* **2018**, *28*, No. 1803168.

- (7) Pyo, S.; Lee, J.; Kim, W.; Jo, E.; Kim, J. Multi-Layered, Hierarchical Fabric-Based Tactile Sensors with High Sensitivity and Linearity in Ultrawide Pressure Range. *Adv. Funct. Mater.* **2019**, *29*, No. 1902484.

- (8) Yang, Y.; Shi, L.; Cao, Z.; Wang, R.; Sun, J. Strain Sensors with a High Sensitivity and a Wide Sensing Range Based on a Ti3C2Tx-(Mxene) Nanoparticle–Nanosheet Hybrid Network. *Adv. Funct. Mater.* **2019**, *29*, No. 1807882.

- (9) Cooper, C. B.; Arutselvan, K.; Liu, Y.; Armstrong, D.; Lin, Y.; Khan, M. R.; Genzer, J.; Dickey, M. D. Stretchable Capacitive Sensors of Torsion, Strain, and Touch Using Double Helix Liquid Metal Fibers. *Adv. Funct. Mater.* **2017**, *27*, No. 1605630.

- (10) Chen, S.; Song, Y.; Ding, D.; Ling, Z.; Xu, F. Flexible and Anisotropic Strain Sensor Based on Carbonized Crepe Paper with Aligned Cellulose Fibers. *Adv. Funct. Mater.* **2018**, *28*, No. 1802547.

- (11) Trung, T. Q.; Lee, N. E. Flexible and Stretchable Physical Sensor Integrated Platforms for Wearable Human-Activity Monitoring and Personal Healthcare. *Adv. Mater.* **2016**, *28*, 4338–4372.

- (12) Roh, E.; Hwang, B. U.; Kim, D.; Kim, B. Y.; Lee, N. E. Stretchable, Transparent, Ultrasensitive, and Patchable Strain Sensor for Human-Machine Interfaces Comprising a Nanohybrid of Carbon Nanotubes and Conductive Elastomers. *ACS Nano* **2015**, *9*, 6252–6261.

- (13) Liu, X.; Su, G.; Guo, Q.; Lu, C.; Zhou, T.; Zhou, C.; Zhang, X. Hierarchically Structured Self-Healing Sensors with Tunable Positive/Negative Piezoresistivity. *Adv. Funct. Mater.* **2018**, *28*, No. 1706658.

- (14) Agarwala, S.; Goh, G. L.; Dinh Le, T. S.; An, J.; Peh, Z. K.; Yeong, W. Y.; Kim, Y. J. Wearable Bandage-Based Strain Sensor for Home Healthcare: Combining 3d Aerosol Jet Printing and Laser Sintering. *ACS Sens.* **2019**, *4*, 218–226.

- (15) Yamada, T.; Hayamizu, Y.; Yamamoto, Y.; Yomogida, Y.; Izadi-Najafabadi, A.; Futaba, D. N.; Hata, K. A Stretchable Carbon Nanotube Strain Sensor for Human-Motion Detection. *Nat. Nanotechnol.* **2011**, *6*, 296–301.

- (16) Ryu, S.; Lee, P.; Chou, J. B.; Xu, R.; Zhao, R.; Hart, A. J.; Kim, S.-G. Extremely Elastic Wearable Carbon Nanotube Fiber Strain Sensor for Monitoring of Human Motion. *ACS Nano* **2015**, *9*, 5929–5936.

- (17) Wu, X.; Han, Y.; Zhang, X.; Lu, C. Spirally Structured Conductive Composites for Highly Stretchable, Robust Conductors and Sensors. *ACS Appl. Mater. Interfaces* **2017**, *9*, 23007–23016.

- (18) Amjadi, M.; Pichitpajongkit, A.; Lee, S.; Ryu, S.; Park, I. Highly Stretchable and Sensitive Strain Sensor Based on Silver Nanowire-Elastomer Nanocomposite. *ACS Nano* **2014**, *8*, 5154–5163.

- (19) Liu, Z.; Qi, D.; Hu, G.; Wang, H.; Jiang, Y.; Chen, G.; Luo, Y.; Loh, X. J.; Liedberg, B.; Chen, X. Surface Strain Redistribution on Structured Microfibers to Enhance Sensitivity of Fiber-Shaped Stretchable Strain Sensors. *Adv. Mater.* **2018**, *30*, No. 1704229.

- (20) Nur, R.; Matsuhisa, N.; Jiang, Z.; Nayeem, M. O. G.; Yokota, T.; Someya, T. A Highly Sensitive Capacitive-Type Strain Sensor Using Wrinkled Ultrathin Gold Films. *Nano Lett.* **2018**, *18*, 5610–5617.

- (21) Kang, D.; Pikhitsa, P. V.; Choi, Y. W.; Lee, C.; Shin, S. S.; Piao, L.; Park, B.; Suh, K. Y.; Kim, T. I.; Choi, M. Ultrasensitive Mechanical Crack-Based Sensor Inspired by the Spider Sensory System. *Nature* **2014**, *516*, 222–226.

(22) Yang, T.; Li, X.; Jiang, X.; Lin, S.; Lao, J.; Shi, J.; Zhen, Z.; Li, Z.; Zhu, H. Structural Engineering of Gold Thin Films with Channel Cracks for Ultrasensitive Strain Sensing. *Mater. Horiz.* **2016**, *3*, 248–255.

(23) Han, Z.; Liu, L.; Zhang, J.; Han, Q.; Wang, K.; Song, H.; Wang, Z.; Jiao, Z.; Niu, S.; Ren, L. High-Performance Flexible Strain Sensor with Bio-Inspired Crack Arrays. *Nanoscale* **2018**, *10*, 15178–15186.

(24) Peng, S.; Wu, S.; Yu, Y.; Blanloeuil, P.; Wang, C. H. Nano-Toughening of Transparent Wearable Sensors with High Sensitivity and a Wide Linear Sensing Range. *J. Mater. Chem. A* **2020**, *8*, 20531–20542.

(25) Amjadi, M.; Turan, M.; Clementson, C. P.; Sitti, M. Parallel Microcracks-Based Ultrasensitive and Highly Stretchable Strain Sensors. *ACS Appl. Mater. Interfaces* **2016**, *8*, 5618–5626.

(26) Zhou, J.; Xu, X.; Xin, Y.; Lubineau, G. Coaxial Thermoplastic Elastomer-Wrapped Carbon Nanotube Fibers for Deformable and Wearable Strain Sensors. *Adv. Funct. Mater.* **2018**, *28*, No. 1705591.

(27) Ohring, M. *Materials Science of Thin Films*; Elsevier, 2001.

(28) Smith, D. L.; Hoffman, D. W. Thin-Film Deposition: Principles and Practice. *Phys. Today* **1996**, *49*, 60.

(29) Lee, J.; Kim, S.; Lee, J.; Yang, D.; Park, B. C.; Ryu, S.; Park, I. A Stretchable Strain Sensor Based on a Metal Nanoparticle Thin Film for Human Motion Detection. *Nanoscale* **2014**, *6*, 11932–11939.

(30) Graz, I. M.; Cotton, D. P. J.; Lacour, S. P. Extended Cyclic Uniaxial Loading of Stretchable Gold Thin-Films on Elastomeric Substrates. *Appl. Phys. Lett.* **2009**, *94*, No. 071902.

(31) Hsieh, H. H.; Hsu, F. C.; Chen, Y. F. Energetically Autonomous, Wearable, and Multifunctional Sensor. *ACS Sens.* **2018**, *3*, 113–120.

(32) Yang, Z.; Pang, Y.; Han, X. L.; Yang, Y.; Ling, J.; Jian, M.; Zhang, Y.; Yang, Y.; Ren, T. L. Graphene Textile Strain Sensor with Negative Resistance Variation for Human Motion Detection. *ACS Nano* **2018**, *12*, 9134–9141.